INTELLIGENT NUMERICAL METHOD FOR STUDYING MAXWELL WILLIAMSON NANOFLUID FLOW WITH ACTIVATION ENERGY

Eman Fayz A. Alshehery
PhD student, Department of Mathematics, Faculty of Science, King Abdulaziz University, Jeddah 21589, Saudi Arabia
Lecturer, Department of Mathematics, Faculty of Science, University of Bisha, Bisha 61922, Saudi Arabia
eabdulrahmanalshehery@stu.kau.edu.sa

Eman Salem Alaidarous
Professor, Department of Mathematics, Faculty of Science, King Abdulaziz University, Jeddah 21589, Saudi Arabia
ealaidarous@kau.edu.sa

Rania. A. Alharbey
Professor, Department of Mathematics, Faculty of Science, King Abdulaziz University, Jeddah 21589, Saudi Arabia
rania.math@gmail.com

Muhammad Asif Zahoor Raja
Professor, Future Technology Research Center, National Yunlin University of Science and Technology, Douliou, Yunlin 64002, Taiwan.

Abstract

The use of artificial intelligence and its techniques has become increasingly widespread in recent times. It is being used to solve stiff non-linear equations. Additionally, nanofluids play a pivotal role in studying heat transfer. All of this was the motivation for doing this work. This work investigates a two-dimensional magnetohydrodynamic stretched flow (2D-MHDSF) of Maxwell Williamson nanofluid (MWNF) affected by bioconvection and activation energy numerically through Levenberg-Marquardt backpropagation method (LMBM)-based artificial neural network approach. The mathematical formulation for the problem was obtained through non-linear partial differential equations (PDEs). The leading PDEs were transmitted into non-linear ordinary differential equations by similarity transformation variables. The reference results for the 2D-MHDSF-MWNF model are produced by the Lobatto IIIA method through different scenarios of specific parameters for the flow velocity, fluid temperature, nanoparticle concentration, and motile density profiles. Using obtained results as a dataset to apply the testing, training, and validation steps of the suggested LMBM for the 2D-MHDSF-MWNF model. The mean squared error, analysis of regression, and error histograms are presented to prove the efficiency and precision of the proposed method. The numerical results of LMBM are displayed as a study of the effects of different physical factors on flow dynamics for 2D-MHDSF-MWNF.

Keywords

Nanofluid, Artificial Neural Network, Activation Energy, Bioconvection

1. Introduction

A nanofluid is a fluid that consists of nanoparticles, or particles that are nanometers in size. A tiny number of nanoparticles are suspended in base fluids like water, ethylene glycol, etc. to create nanofluids. In 1995 Choi first used the concept of "nanofluid" in his innovative article, at the Winter Annual Conference of the American Society of Mechanical Engineers (Choi & Eastman, 1995). As a result of their superior thermal qualities, nanofluids are increasingly being employed as coolants in many types of heat transfer equipment, including heat transfer, electronic cooling systems, and radiators. To improve heat transfer, Buongiorno (Buongiorno, 2006) proposed the Brownian motion effect, uncommon two-slip phenomena, and thermophoresis. Many studies have examined heat transport across different surfaces. The unstable magnetohydrodynamic stream of a hybrid nanofluid influenced by heat and mass transport is investigated by (Sreedevi, Sudarsana Reddy, & Chamkha, 2020). (Esfe, Esfandeh, &

Hosseinizadeh, 2020) studied the immersion of nanofluids to improve the recovery of oil in a 2D varied geometry. (Sharif et al., 2020) analyzed the Eyring nanofluid stream impacted by activation energy and bioconvection. The effect of heat transport with a vertical surface on a nanofluid stream is studied by (Alim, Alam, & Hossain, 2008). The impact of Stefan blowing conditions on ferromagnetic fluid stream across a sheet is illustrated by (Gowda, Kumar, Prasannakumara, Nagaraja, & Gireesha, 2021).

The study of the behavior of electrically conducting fluids in the presence of magnetic fields, including plasmas, liquid metals, and salt water, is known as magnetohydrodynamics (MHD). It integrates concepts from fluid dynamics with magnetism to explain phenomena such as the behavior of plasma in laboratory and astrophysical environments, the creation of electric electrical currents through conductive fluids, and the collaboration of the magnetic field with fluid motion. Many studies have examined the characteristics of MHD in recent decades. (Gul et al., 2021) illustrated the MHD unstable flow of nanofluid across the stretchable rotating surface. (Rasool, Chamkha, Muhammad, Shafiq, & Khan, 2020) investigated numerical study for the Casson MHD nanofluid across a non-linear stretching sheet with Darcy-Forchheimer law. The MHD thin-film Oldroyd-B fluid flow under the impact of bio-convection and activation energy is reviewed by (Ahmad et al., 2021). (Chu et al., 2020) illustrated the influence of gyrotactic microorganisms on the MHD flow of third-grade fluid across a sheet.

The model used to describe the features of the non-Newtonian fluid is called the Maxwell model. This model exhibits viscous flow over long-time scales and enhanced elastic resistance to quick deformations. In 1867, a Scottish mathematician James Clerk Maxwell presented the model and it is also called Maxwell fluid. Recently, Maxwell nanofluid flow models have been studied by many researchers. The Maxwell nanofluid flow across a linear stretchable surface is evaluated by Sharma et al. (Sharma, Hussain, Raju, Seth, & Chamkha, 2020). (Ahmed, Khan, & Ahmad, 2020) illustrated the Maxwell nanofluid stream on a stretched rotating surface impacted by a chemical reaction and radiative heat flux. By employing fractional derivatives (Abro, Soomro, Atangana, & Gómez-Aguilar, 2020) presented the thermal behavior of Maxwell nanofluid with the usual kernel. The Marangoni Maxwell nanofluid stream across a rotating surface is affected by entropy generation and Arrhenius activation energy studied numerically by (Alsallamiet al., 2022). Williamson fluid is described as a non-Newtonian fluid having shear thinning properties that is when the viscosity is decreasing, the rate of shear stress is increasing.

In 1929, the scientist Williamson proposed the Williamson simulation, which was subsequently investigated by other researchers. The peristaltic Williamson fluid flow subject to the magnetic is reviewed by (Rashid, Ansar, & Nadeem, 2020). (Noreen, Waheed, Lu, & Hussanan, 2020) analyzed the heat transfer properties for electro-osmotic Williamson fluid flow in the microchannel. The Williamson MHD nanofluid stream between rotating disks with a porous medium under the effect of bioconvection was explored by (Bhatti, Arain, Zeeshan, Ellahi, & Doranehgard, 2022). The heat and mass transmission for the three-dimensional mixed convective radiative stream of Williamson nanofluid is investigated by (Ahmad, Faisal, Javed, Mustafa, & Kiyani, 2022).

The term "bioconvection" refers to the unorganized and unstable movement of microorganisms to the top section of a fluid, where the density is lower. As a result of its upward migration, the fluid will experience both surface instability and asymmetric mass transfer. The relativity of bioconvection at low concentrations has become more important to researchers in the suspension of nanoparticles. Mass transport speeds are accelerated by bioconvection. Consequently, several researchers have studied the mechanics of various bio-convection challenges that provide suspended solid particles. (Kanta Mondal & Pal, 2022) explored the bioconvection nanofluid stream between two stretching rotating plates with entropy creation. The effects of the bioconvection inside nanofluids on the stability of nanoparticles are explored by (Raees, Xu, Sun, & Pop, 2015). (Khan & Makinde, 2014) assumed the gyrotactic microorganisms enhance the concentration of the base fluid in the nanofluid by moving in a determined shape. The radiative squeezing nanofluid stream between two rotating disks subject to bioconvection was illustrated by (Zeeshan, Arain, Bhatti, Alzahrani, & Bég, 2022). (Arain, Zeeshan, Alhodaly, Fasheng, & Bhatti, 2022) analyzed the impact of bioconvection and activation energy on the nanofluid flow across a fixed vertical parallel surface.

Activation energy is the minimum amount of energy desired to initiate a chemical process and to simulate a reaction. In 1889, Arrhenius proposed the concept of "activation energy" for the first time. Applications of activation energy include controlling chemical reactions, fission and fusion reactions, oil reservoirs, geothermal engineering, chemical engineering, food processing, and water emulsions. The activation energy and chemical process have been the subject of a very limited number of studies yet. (Mustafa, Khan, Hayat, & Alsaedi, 2017) investigated the magneto nanofluid's activation energy properties and chemical processes.

(Dhlamini, Kameswaran, Sibanda, Motsa, & Mondal, 2019) found that thermophoresis and Arrhenius activation energy raise the concentration of the chemical types by studying the impact of thermophoresis and activation energy on the mixed convective flow of nanofluid over a heated vertical plate. Using a stretchable sheet with heat generation and Arrhenius activation energy, (Reddy, Reddy, & Bhattacharyya, 2019) examined the three-dimensional non-Newtonian hydromagnetic slip nanofluid flow (Eyring-Powell stream). (Hayat, Khan, Khan, & Alsaedi, 2019) enhanced the investigation of the second law with the Eyring-Powell stream of nanofluid between two rotating disks influenced by activation energy. (Irfan, Khan, Khan, & Gulzar, 2019) considered the stream behavior of a three-dimensional Carreau nanofluid flow with activation energy.

Artificial neural network (ANN) is a groundbreaking new approach to artificial intelligence. It is a standard statistical technique for examining the relations among variables. ANN consists of interconnected layers of processing units that take in data and output results based on previously defined activation functions. An artificial neural network is a highly effective numerical technique due to its higher convergence rate and lower mean square errors. Stiff nonlinear issues in various domains have recently been solved using stochastic numerical techniques based on artificial intelligence. Artificial neural networks are used in these stochastic computing techniques to model approximative solutions. These numerical solvers are widely used in a variety of fields, such as fluidic systems (Lira, Riella, Padoin, & Soares, 2022), petroleum engineering (Khan, Sulaiman, Aljohani, Kumam, & Alrabaiah, 2020), wire coating problem (Khan, Sulaiman, Kumam, & Aljohani, 2021), COVID-19 disease model (Cheema et al., 2020), and heat diffusion (Ahmad, Sulaiman, Alhindi, & Aljohani, 2020). To reduce network error, backpropagation (BP) employs the gradient descent approach, which involves following the defined error curve's gradient in the opposite direction. Paul Werbos created the backpropagation method in 1974. The Levenberg-Marquardt technique is a novel convergence strategy for ANNs to numerically solve various fluid flow problems. Casson MHD nanofluid flow through Darcy-Forchheimer medium porous affected by heat exporter and activation energy is investigated by (Shoaib et al., 2022) through the Levenberg-Marquardt backpropagation method LMBM.

The model of flow 2D-MHDSF-MWNF helps in studying the possibility of improving the thermal conductivity during the flow of different common nanofluids through a study of two different types of nanofluid flows Williamson and Maxwell nanofluids impacted by bioconvection

of micro-organism and activation energy, and this can be used in many applications of thermal engineering and thermal sciences. Therefore, this study aims to analyze the effect of bioconvection and Arrhenius activation energy on the two-dimensional magnetohydrodynamic stretched flow 2D-MHDSF of Maxwell Williamson nanofluid MWNF by using the intelligent numerical method through the Levenberg Marquardt backpropagation method LMBM. The steps of the suggested numerical intelligent computing method are presented below:

- The Levenberg-Marquardt backpropagation method LMBM used to establish numerical intelligent computing for the two-dimensional magnetohydrodynamic stretched flow 2D-MHDSF of Maxwell Williamson nanofluid (MWNF) affected by the activation energy and bioconvection.

- The mathematical formulation for the 2D-MHDSF-MWNF is a system of nonlinear PDEs; then these PDEs are converted into a system of nonlinear ODEs by using similarity transformation.

- The Lobatto IIIA method through the bvp4c package in the MATLAB platform generates a dataset that is used as input and target data in the nftool package in MATLAB to apply an artificial neural network technique ANN which is trained through suggested LMBM for the effects of the numerous physical variables on the flow.

- The graphs of MSE of performance, fitness curve, regression analysis, and histogram error examine the accuracy of the recommended LMBM for 2D-MHDSF-MWNF.

The remaining sections of this study are described as the mathematical model of 2D-MHDSF-MWNF introduced in section 2. In section 3 solution methodology of the suggested technique LMBM is presented. Section 4 involves the validation of the result for different scenarios on velocity, temperature, and concentration profile. Section 5 discusses the conclusion of our study.

2. Mathematical Model

Consider the two-dimensional steady magnetohydrodynamic stream of Maxwell Williamson nanofluid is influenced by Cattaneo–Christov diffusion and Arrhenius activation energy with the bioconvection of microorganisms on a stretchable surface. The geometrical illustration of the problem is given in Figure 1 (Abdal, Siddique, Alrowaili, Al-Mdallal, & Hussain, 2022). In Figure 1, T, C, and N represent the fluid temperature, nanoparticle concentration, and density of the microorganisms close to the surface, respectively. The speeds of fluids stream over the axis x and axis y are u and v. The stretched velocity of slip over the *x*-axis U_w and the stretching

constant D form the wall velocity $U_w = Dx$. In Cartesian coordinates, the problem reflects the fundamental equations of continuity, momentum, energy, concentration, and gyrotactic microorganism concentration.

Figure 1: *Geometrical illustration of flow*
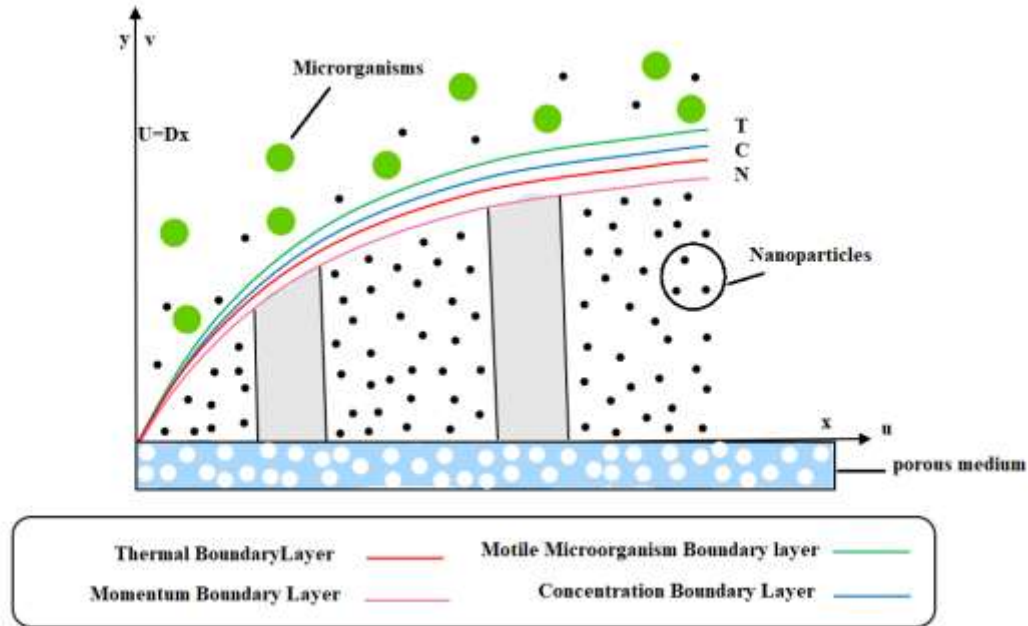
(Source: Self/Authors' Own Illustration)

The governing PDEs of flow formulation are given below ((Sharif et al., 2020), (Abdal et al., 2022), (Hussain, Sharma, Mishra, & Alrashidy, 2020), (Dapra & Scarpi, 2007)).

$$\frac{\partial u}{\partial x} + \frac{\partial v}{\partial y} = 0, \tag{1}$$

$$u\frac{\partial u}{\partial x} + v\frac{\partial u}{\partial y} = v\frac{\partial^2 u}{\partial y^2} + \sqrt{2}v\Gamma\frac{\partial u}{\partial y}\frac{\partial^2 u}{\partial y^2} - \frac{\sigma B_0{}^2 u}{\rho} - \frac{v}{k'}u \tag{2}$$

$$- \lambda_1\left[u^2\frac{\partial^2 u}{\partial x^2} + v^2\frac{\partial^2 u}{\partial y^2} + 2uv\frac{\partial^2 u}{\partial y\partial x}\right]$$

$$+ \left(\rho\beta(T - T_\infty)(1 - C_\infty) - g(\rho_p - \rho)(C - C_\infty)\right.$$

$$\left. - g\gamma(N - N_\infty)(\rho_m - \rho)\right)\left(\frac{1}{\rho}\right),$$

$$u\frac{\partial T}{\partial x} + v\frac{\partial T}{\partial y} = \alpha\frac{\partial^2 T}{\partial y^2} + \frac{\rho_p C_p}{\rho C}\left[D_B\frac{\partial T}{\partial y}\frac{\partial C}{\partial y} + \left(\frac{\partial T}{\partial y}\right)^2\frac{D_T}{T_\infty}\right] \quad (3)$$

$$+ \tau_1\left[u\frac{\partial T}{\partial x}\frac{\partial u}{\partial x} + v\frac{\partial T}{\partial x}\frac{\partial v}{\partial x} + u\frac{\partial T}{\partial x}\frac{\partial v}{\partial x} + v\frac{\partial T}{\partial x}\frac{\partial u}{\partial y} + 2uv\frac{\partial^2 T}{\partial x\partial y} + u^2\frac{\partial^2 T}{\partial x^2}\right.$$

$$\left.+ v^2\frac{\partial^2 T}{\partial y^2}\right]$$

$$v\frac{\partial C}{\partial y} + u\frac{\partial C}{\partial x} = D_B\frac{\partial^2 C}{\partial y^2} + \frac{D_T}{T_\infty}\frac{\partial^2 T}{\partial y^2} - (Kr)^2(C_w - C_\infty)\left(\frac{T}{T_\infty}\right)^m \exp\left(\frac{-E_a}{k_2 T}\right), \quad (4)$$

$$v\frac{\partial N}{\partial y} + u\frac{\partial N}{\partial x} + bW_e\frac{\partial}{\partial y}\left(\frac{\partial C}{\partial y}\frac{n}{\Delta C}\right) = D_m\frac{\partial^2 N}{\partial y^2}. \quad (5)$$

$$U_w = u = Dx, v = v_w, C - C_w(x) = 0, N - N_w(x) = 0, T - T_w(x) = 0, \text{ at } y = 0, \quad (6)$$

$$u \to 0, C \to C_\infty, N \to N_\infty, T \to T_\infty, \text{ as } y \to \infty$$

Applying transformation for similarity

$$\eta = \sqrt{\frac{D}{v}}y, u = Dxf'(\eta), v = -\sqrt{Dv}f(\eta), \theta(\eta) = \frac{T - T_\infty}{T_w - T_\infty}, \phi(\eta) = \frac{C - C_\infty}{C_w - C_\infty}, \quad (7)$$

$$\chi(\eta) = \frac{N - N_\infty}{N_w - N_\infty}.$$

Here, in Eq (2) λ_1 is the Maxwell fluid parameter and Γ is the Williamson fluid parameter, so if $\lambda_1 = 0$ and $\Gamma \neq 0$, it represents the Williamson fluid flow. But if $\lambda_1 \neq 0$ and $\Gamma = 0$, then it is Maxwell fluid flow. Since, there is an identical balance in Eq (1), Eqs (2)-(5) converted to

$$f''' + ff'' - f'^2 - \beta(f^2 f''' - 2ff'f'') - (M + Kp)f' + \lambda f''f''' \quad (8)$$
$$+ \omega(\theta - Nr\phi - Rb\chi) = 0,$$

$$\theta'' + Pr f \theta' + \frac{Nc}{Le}\theta'\phi' + \frac{Nc}{Le * Nb}\theta'^2 + b(f^2\theta'' + ff'\theta') = 0, \quad (9)$$

$$\phi'' + Sc(f\phi') + \left(\frac{1}{Nb}\right)\theta'' - ScA\phi(1 + \delta\theta)^m \exp\left(\frac{-E}{1 + \delta\theta}\right) = 0, \quad (10)$$

$$\chi'' + Lb(f\chi') - Pe[\phi''(\chi + \Omega) + \chi'\phi'] = 0. \quad (11)$$

With boundary conditions

$$f = S, f' = 1, \theta = 1, \phi = 1, \chi = 1, \quad \text{if } \eta = 0$$
$$f' \to 0, \theta \to 0, \phi \to 0, \chi \to 0, \quad \text{if } \eta \to \infty \quad (12)$$

Where $\beta = \lambda_1 D$ is Deborah number, $M = \frac{\sigma B_0^2}{D\rho}$ is magnetic parameter, $K_p = \frac{\upsilon}{k_1 D}$ is porosity parameter, λ is non-Newtonian Williamson parameter, $\omega = \frac{\beta_1 g(1-C_\infty)(T_w-T_\infty)}{D^2 x}$ is mixed convection, $Nr = \frac{(\rho_p-\rho)(C_w-C_\infty)}{\beta_1\rho(1-C_\infty)(T_w-T_\infty)}$ is buoyancy ratio, $Rb = \frac{(\rho_m-\rho)\gamma N_\infty}{(1-C_\infty)\rho\beta T_\infty}$ is Rayleigh number, $Pr = \frac{\upsilon}{\alpha}$ is Prandtl number, $Nb = \frac{D_B T_\infty(C_w-C_\infty)}{D_T(T_w-T_\infty)}$ is diffusivity ratio, $Le = \frac{\alpha}{D_B}$ is Lewis number, $b = \tau_1 D$ is thermal relaxation constant, $Sc = \frac{\upsilon}{D_B}$ is Schimdt number, $A = \frac{K_r^2}{D}$ is reaction rate, m is fitted number, $\delta = \frac{T_w-T_\infty}{T_\infty}$ is temperature ratio, $E = \frac{E_a}{k_2 T_\infty}$ is activation energy, $Lb = \frac{\upsilon}{D_m}$ is bio-convection Lewis number, $Pe = \frac{b_1 W_e}{D_m}$ is Peclet number, $\Omega = \frac{N_\infty}{N_w-N_\infty}$ is microorganism concentration ratio, and $S = \frac{-v_w}{\sqrt{D\upsilon}}$ is suction/injection parameter.

Also, the physical quantities are ((Abdal et al., 2022), (Krishnamurthy, Prasannakumara, Gireesha, & Gorla, 2016))

$$Cf_x = \frac{\tau_w}{\rho U^2 w}, Nu_x = \frac{x q_w}{k(T_w - T_\infty)},$$
$$Sh_x = \frac{x q_m}{D_B(C_w - C_\infty)}, Nn_x = \frac{x q_n}{D_m(N_w - N_\infty)}. \quad (13)$$

Here, Cf_x represents skin friction coefficient, τ_w shear stress, Nu_x local Nusselt number, q_w surface heat flux, Sh_x local Sherwood number, q_m surface mass flux, Nn_x local density of microorganism, and q_n motile microorganism flux. Therefore

$$\tau_w = \mu(1+\beta)\left(1 + \frac{\Gamma}{2}\frac{\partial u}{\partial y}\right)\frac{\partial u}{\partial y}, q_w = -K\frac{\partial T}{\partial y}, q_m = -D_B\frac{\partial C}{\partial y}, q_n = -D_m\frac{\partial N}{\partial y}. \quad (14)$$

By using the given similarity transformation to these quantities,

$$Cf_x(Re_x)^{-1/2} = (1+\beta)\left(f''(0) + \frac{\lambda}{2}f''(0)^2\right), Nu_x(Re_x)^{-1/2} = -\theta'(0),$$

$$Sh_x(Re_x)^{-1/2} = -\phi(0), Nn_x(Re_x)^{-1/2} = -\chi'(0). \tag{15}$$

Here, $(Re_x) = \frac{xU_w}{v}$ denotes local Reynolds number.

3. Solution Methodology

The solution methodology in this study is implemented in two phases. Firstly, the numerical solutions for the mathematical formulation of two-dimensional magnetohydrodynamic stretched flow 2D-MHDSF of Maxwell Williamson nanofluid MWNF are found by solving ODEs (8)-(11) with boundary conditions (12) for different scenarios of physical parameters through the Lobatto IIIA method by using bvp4c package in MATLAB platform. Secondly, these solutions were used as reference data through the nftool package in the MATLAB platform to apply the Levenberg Marquardt backpropagation method LMBM to investigate the approximate solution of 2D-MHDSF-MWNF through determining the number of neurons, training, testing, and validation data.

The approximate solution for two-dimensional magnetohydrodynamic stretched flow (2D-MHDSF) of Maxwell Williamson nanofluid MWNF which is obtained through nftool for six scenarios by changing the parameter of magnetic variable (*M*), thermal relaxation constant (*b*), Prandtl number (*Pr*), activation energy (*E*), the reaction rate (*A*), and bio-convection Lewis number (*Lb*) all through various four cases with constant values of $\beta = 0.5, \lambda = 0.1, M = 0, Kp = 0, \omega = 0.1, Nr = 1, Rb = 1, Pr = 0.5, Le = 0.1, Nbt = 1, b = 1, Sc = 1, A = 0.1, \delta = 1, E = 1, Lb = 0.1, Pe = 0, \Omega = 0.05, S = 1, Nc = 0.1, m = 0.1$. Table 1 shows the details of every scenario of the two-dimensional magnetohydrodynamic stretched flow 2D-MHDSF of Maxwell Williamson nanofluid MWNF. The nftool package in MATLAB software is used to create the LMBM, which uses ten neurons, 80% of the data set for the training step, 10% for the validation step, and 10% for the testing step. A form of an artificial neural network for 2D-MHDSF-MWNF is displayed in Figure 2.

The accuracy of LMBM is analyzed using a regression profile, mean squared error of the performance and histogram error. The obtained solution by LMBM which analyzes the impact of different physical parameters on the velocity $f'(\eta)$, temperature $\theta(\eta)$, concentration fluid (η), and motile density $\chi(\eta)$ profiles is investigated.

Figure 2: *A form of artificial neural network for MHDSF-MWNF*
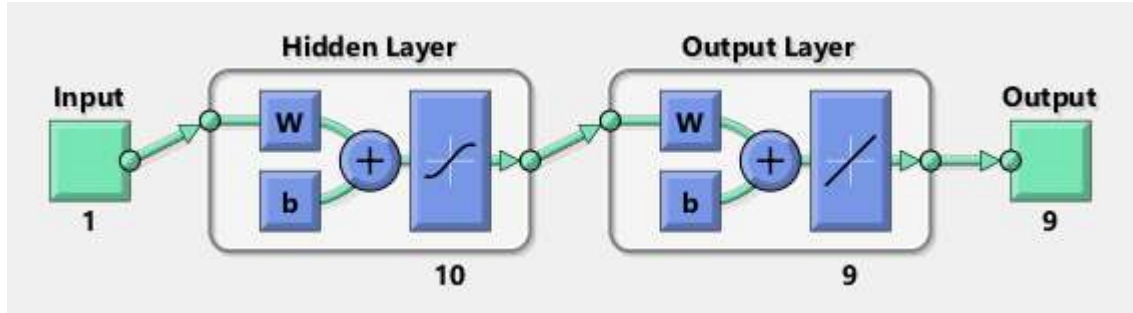
(Source: Self/Authors' Own Illustration)

Table 1 *The values of different parameters of 2D-MHDSF-MWNF*

Scenario	Physical parameters	Profile	Case1	Case2	Case3	Case4
1	M	$f'(\eta)$	0.0	0.3	0.6	0.9
		$\theta(\eta)$	0.0	0.3	0.6	0.9
		$\phi(\eta)$	0.0	0.3	0.6	0.9
		$\chi(\eta)$	0.0	0.3	0.6	0.9
2	b	$\theta(\eta)$	1.0	2.0	3.0	4.0
3	Pr	$\theta(\eta)$	0.5	1.0	1.5	2.0
4	E	$\phi(\eta)$	1.0	2.0	3.0	4.0
5	A	$\phi(\eta)$	0.1	0.5	1.0	1.5
6	Lb	$\chi(\eta)$	0.1	0.2	0.3	0.4

(Source: Self/Authors' Own Illustration)

4. Results and Discussion

Figures 3-7 show the graphical statical results which measure the accuracy LMBM of 2D-MHDSF-MWNF for a variety of cases and scenarios through the examine the errors and relation between the target data (the solution by Lobatto IIIA) and the output data (the solution by LMBM).
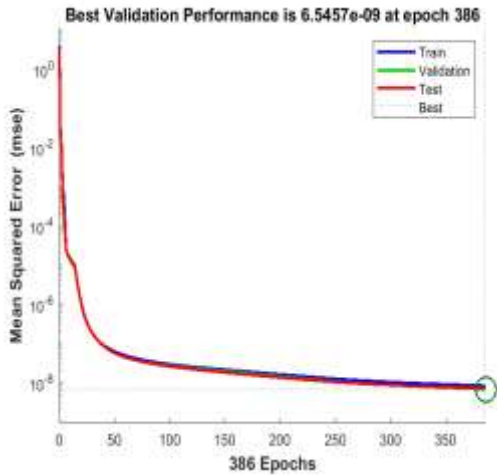
The mean square error MSE of performance for scenarios 2, 5, and 6 with case 1, for scenarios 1 and 4 with case 2, and scenario 3 with case 4 of 2D-MHDSF-MWNF is displayed in Figure 3. The mean square errors 10^{-10}, 10^{-9}, 10^{-9}, 10^{-9}, 10^{-9}, and 10^{-9} at 963, 395, 280, 376, 386, and 523 epochs, respectively, have the greatest performance. The training state outcomes for scenarios 2, 3, and 5 with case 2, for scenario 1 with case 1, and scenarios 4 and 6 with case 4 are shown in Figure 4. Figures 4(a-f) exhibit the convergence of the designed LMBM for 2D-MHDSF-

MWNF through Mu parameter values (10^{-9}, 10^{-8}, 10^{-9}, 10^{-8}, 10^{-9}, and 10^{-9}) and the gradient results ($9.9 \times 10^{-8}, 9.9 \times 10^{-8}, 9.8 \times 10^{-8}, \ 9.9 \times 10^{-8}, 9.9 \times 10^{-8},$ and 9.9×10^{-8}).

The error histogram for scenarios 2 and 5 with case 2, for scenarios 3 and 6 with case 3, for scenario 4 with case 4, and scenario 1 with case 1 is demonstrated in Figure 5. Figures 5(a-f) show the error histogram for the different scenarios with different cases previously mentioned as $-1.9 \times 10^{-5}, \ -5.8 \times 10^{-5}, \ 2.22 \times 10^{-6}, \ -2.8 \times 10^{-5}, 9.22 \times 10^{-6},$ and 1.68×10^{-5}. The regression analysis for scenario 1 with case 1, for scenarios 2 and 5 with case 3, for scenario 3 with case 2, and scenarios 4 and 6 with case 4 is presented in Figure 6. The linear correlation between target data and output data is given through the regression. Figure 6 shows the LMBM for 2D-MHDSF-MWNF is accurate because the correlation value *R=1* for training, testing, validation, and all. Figure 7 introduces the function fit curve of validation, testing, and training processes of scenarios 3, 4, and 5 with case 2, for scenarios 1 and 2 with case 4, and scenario 6 with case 1.

Figure 3: *Mean Square Error (MSE) for LMBM for 2D-MHDSF-MWNF*

a) Mean Squared Error for S1/C2

b) Mean Squared Error for S2 /C1

c) Mean Squared Error for S3/C4
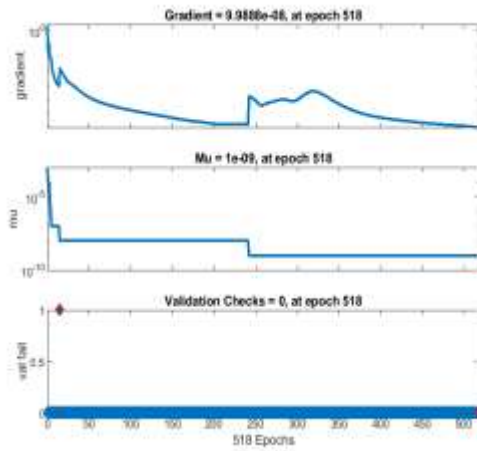

d) Mean Squared Error for S4/C2
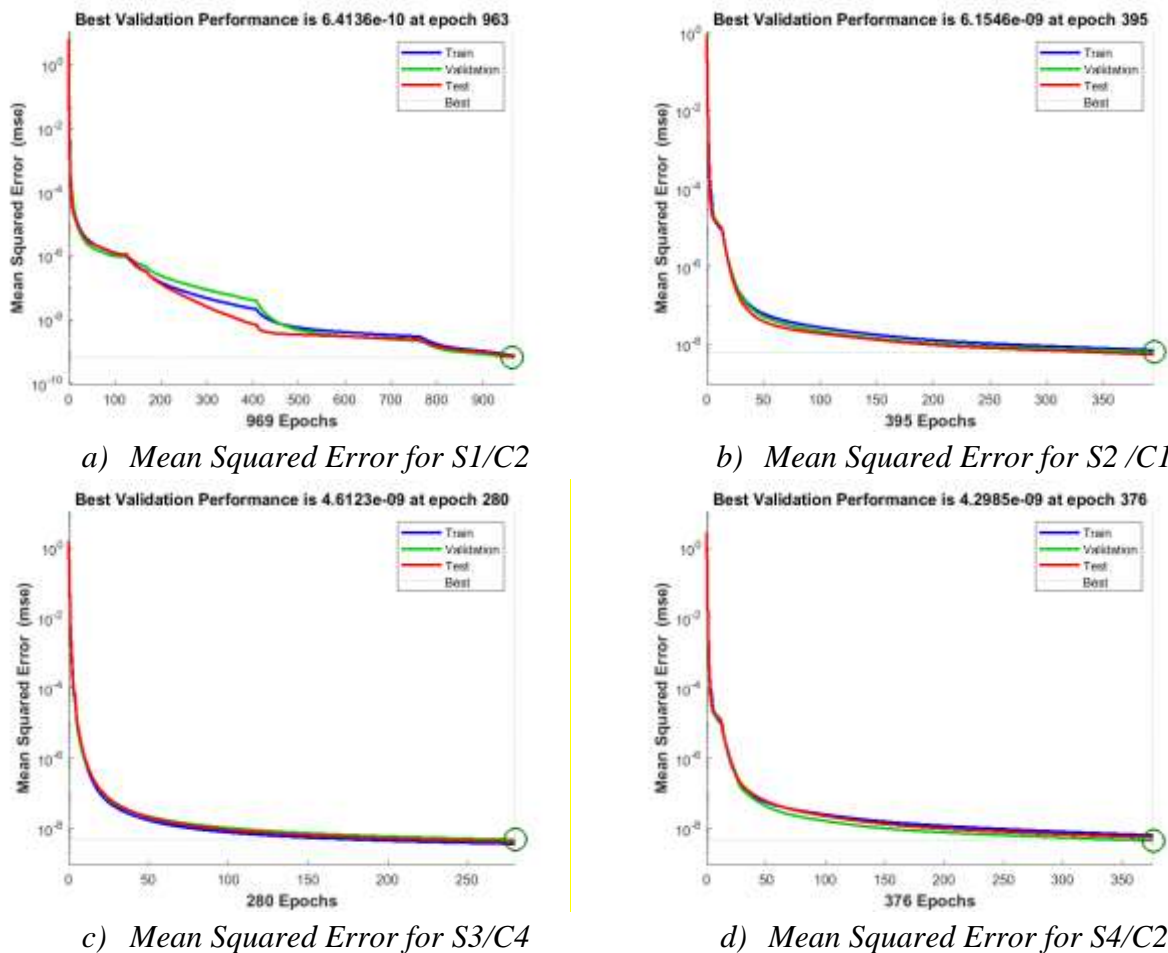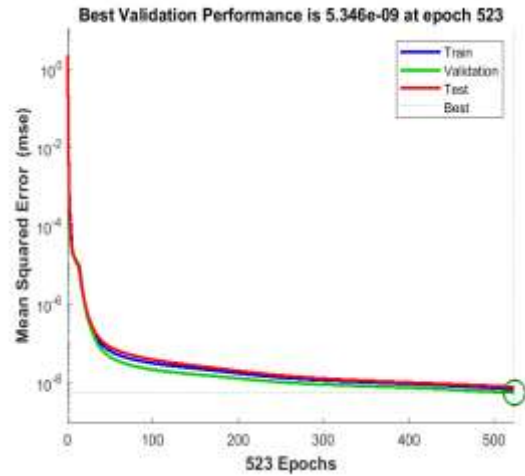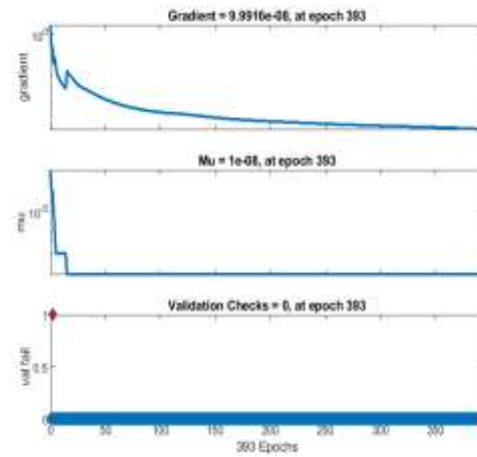
e) Mean Squared Error for S5/C1   *f) Mean Squared Error for S6 /C1*

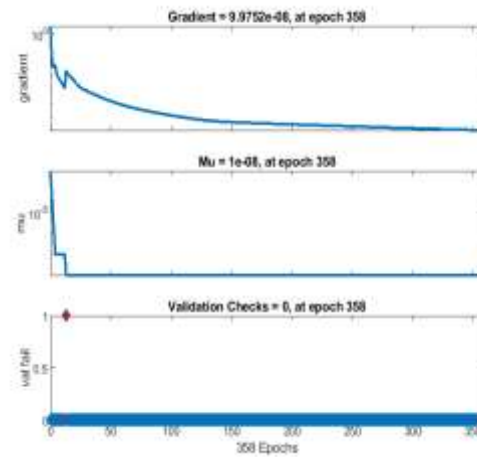(Source: Self/Authors' Own Illustration)
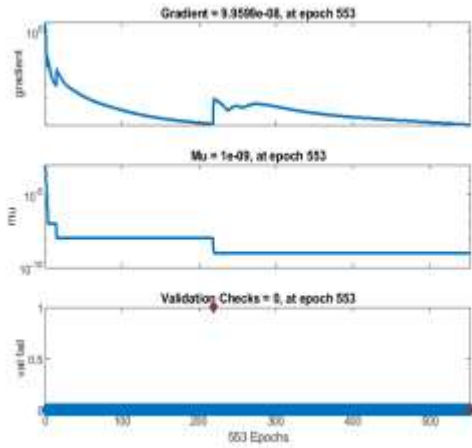
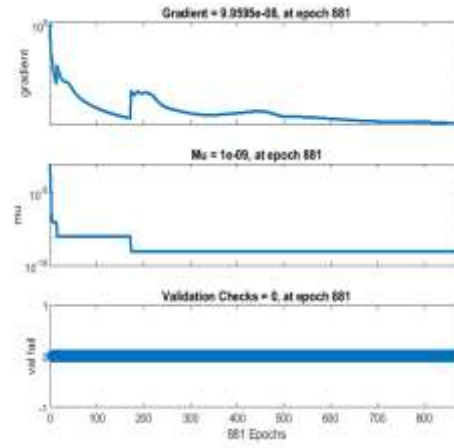**Figure 4:** *Gradient of LMBM for 3D-MHDSF-MWNF*

a) Training state for S1/ C1   *b) Training state for S2/ C2*
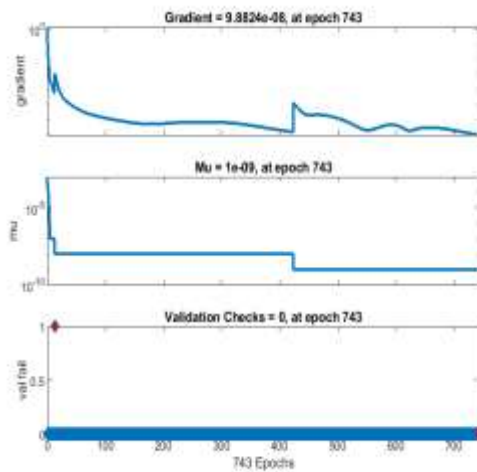
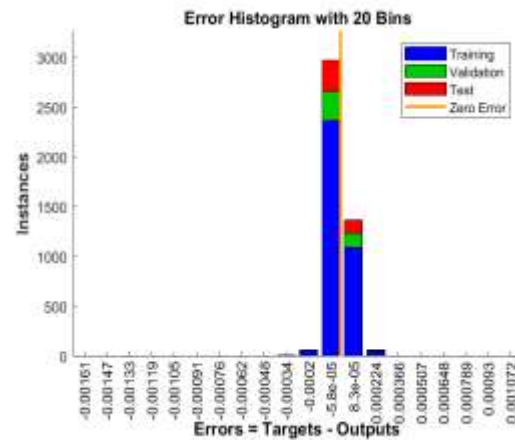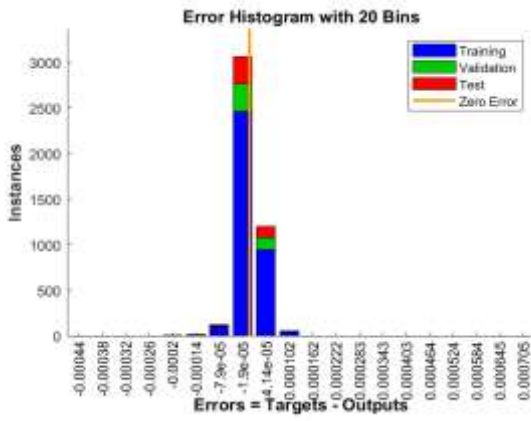|	
c) Training state for S3/ C2	*d) Training state for S4/ C4*

e) Training state for S5/ C2	*f) Training state for S6/ C4*

(Source: Self/Authors' Own Illustration)

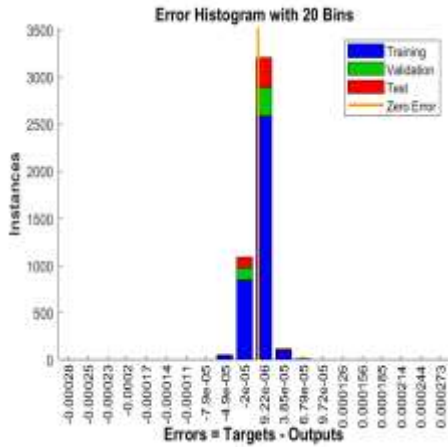**Figure 5:** *Error histogram of LMBM for 2D-MHDSF-MWNF*

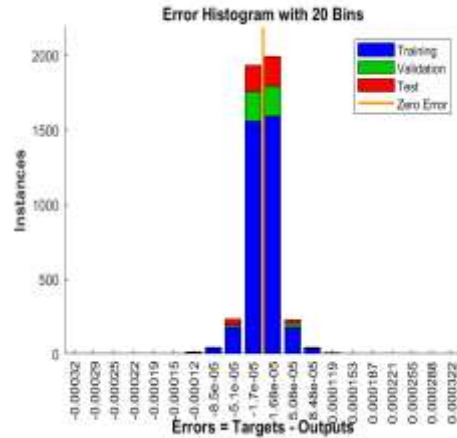|	
a)* *Error histogram about S1/ C1	***b)* *Error histogram about S2/ C2***
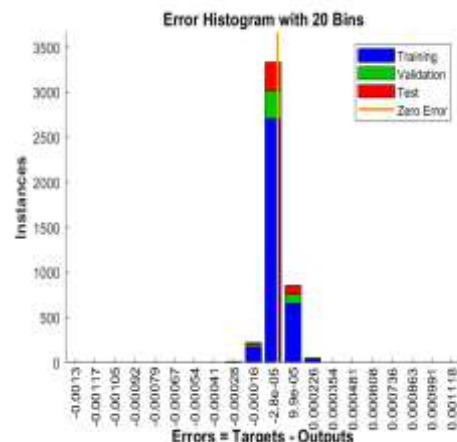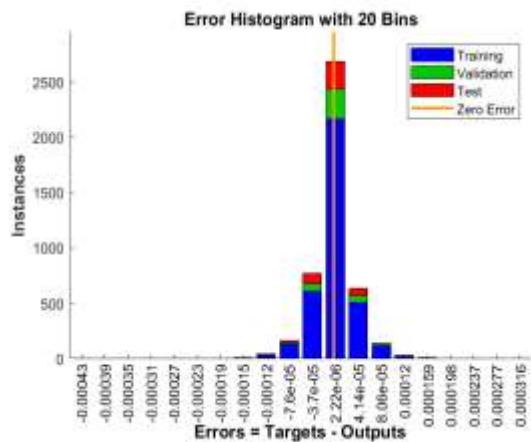
c) *Error histogram about S3/C3*   *d)* *Error histogram about S4/C4*

e) *Error histogram about S5/ C2*   *f)* *Error histogram about S6/ C3*

(Source: Self/Authors' Own Illustration)

Figure 6: *Regression analysis of LMBM for 2D-MHDSF-MWNF*
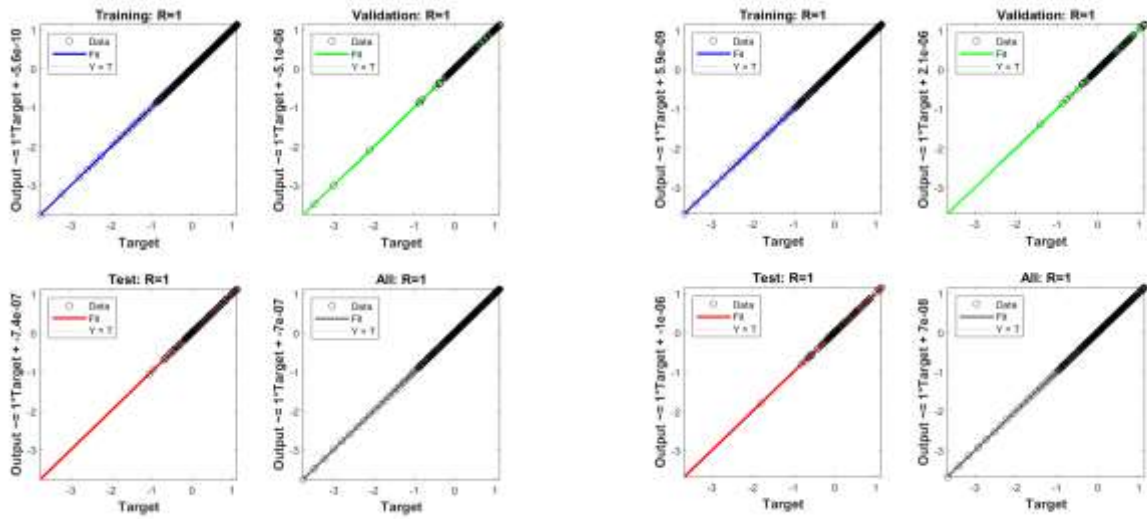
a) *The regression of S1/C1*   *b)* *The regression of S2/C3*
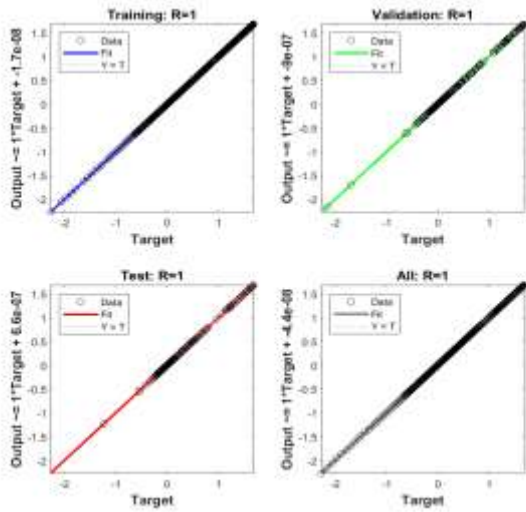
c) The regression of S3/C2

d) The regression of S4/C4

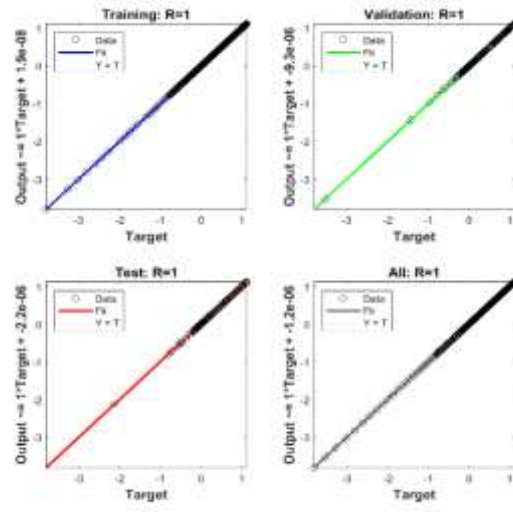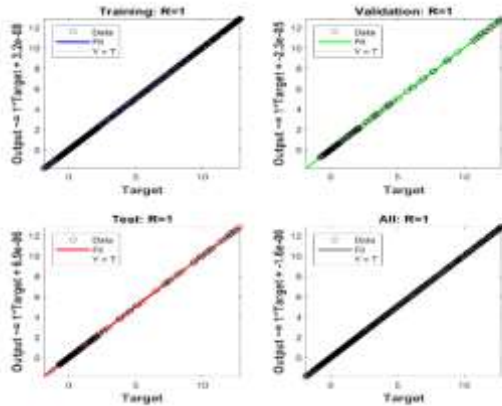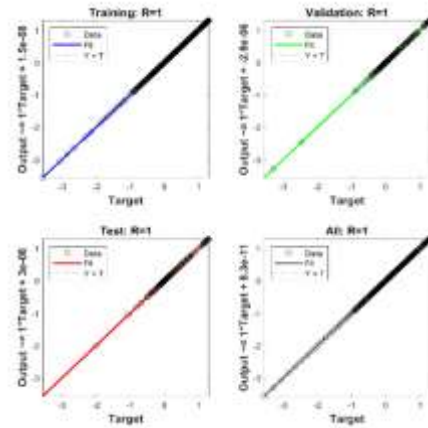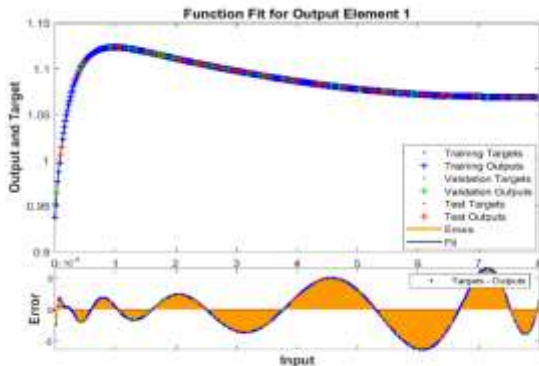*e) The regression of S5/C3*

f) The regression of S6/C4

(Source: Self/Authors' Own Illustration)

Figure 7: *Fitness plot of LMBM for 2D-MHDSF-MWNF*

a) Fitness plot of S1/C4
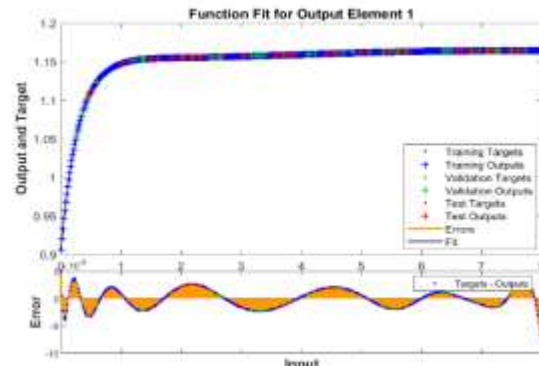
b) Fitness plot of S2/C4
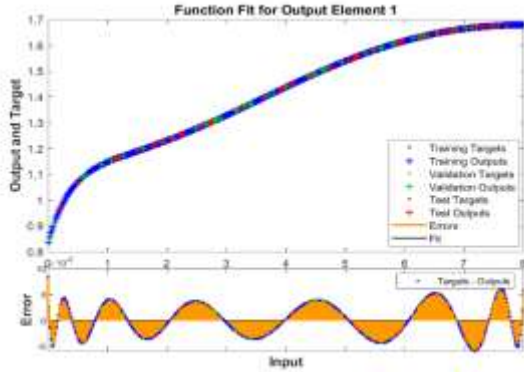
c) Fitness plot of S3/C2
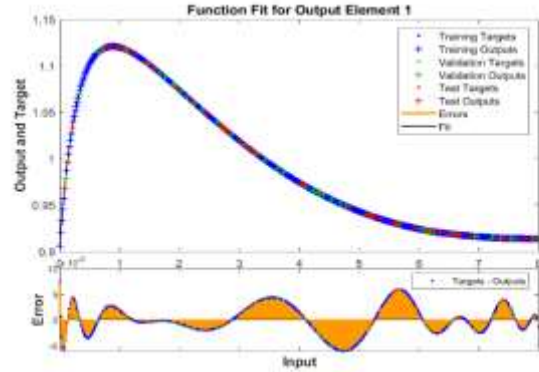
d) Fitness plot of S4/C2
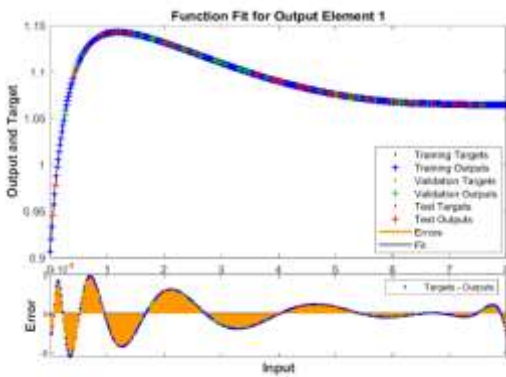
e) Fitness plot of S5/C2
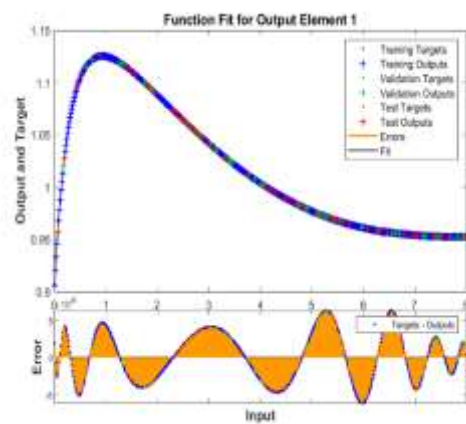
f) Fitness plot of S6/C1

Table 2 shows the numerical results of mean squared error for training, validation, and testing, the performance, gradient, Mu, epochs, and treating period for four cases of ten scenarios.

Table 2 *The numerical results of LMBM for variations of 2D-MHDSF-MWNF*

Scenarios	Cases	Mean Squared Error			Performance	Mu Parameter	Gradient	Epochs	Time
		Training	*Validation*	*Testing*					
S1	**C1**	1.33E-10	2.60E-10	1.46E-10	1.33E-10	1.00E-07	9.99E-08	518	2s
	C2	7.40E-10	6.41E-10	7.03E-10	7.22E-10	1.00E-10	9.76E-06	969	4s
	C3	4.45E-09	4.71E-09	7.57E-09	4.45E-09	1.00E-09	3.06E-06	1000	5s
	C4	2.85E-10	2.41E-10	5.56E-10	2.85E-09	1.00E-09	1.29E-08	1000	6s
S2	**C1**	6.92E-10	6.15E-09	5.31E-09	6.92E-10	1.00E-09	9.99E-09	395	3s
	C2	6.01E-10	4.46E-10	2.52E-10	6.01E-10	1.00E-08	9.99E-07	393	4s
	C3	4.97E-10	3.77E-10	4.98E-10	4.97E-10	1.00E-09	9.98E-09	377	2s

	C4	5.43E-10	3.34E-10	2.88E-10	5.43E-10	1.00E-09	9.96E-09	412	2s
S3	C1	6.91E-09	5.52E-09	7.64E-09	6.91E-09	1.00E-09	9.95E-07	363	1s
	C2	8.28E-10	4.36E-10	5.21E-10	8.28E-10	1.00E-10	9.88E-09	743	3s
	C3	1.30E-09	1.72E-09	1.64E-09	1.30E-09	1.00E-10	3.57E-06	1000	5s
	C4	3.50E-09	4.61E-09	4.01E-09	3.50E-09	1.00E-09	9.97E-09	280	1s
S4	C1	6.23E-10	4.39E-10	4.25E-10	6.23E-10	1.00E-09	1.00E-08	330	3s
	C2	6.15E-08	4.30E-09	5.34E-09	6.15E-08	1.00E-09	9.96E-08	376	3s
	C3	6.37E-10	3.84E-10	3.94E-10	6.37E-10	1.00E-09	9.97E-09	394	3s
	C4	5.83E-09	6.04E-09	5.43E-09	5.83E-09	1.00E-08	9.98E-08	358	1s
S5	C1	7.99E-09	6.55E-09	6.97E-09	7.99E-09	1.00E-08	9.98E-08	386	3s
	C2	2.67E-10	1.88E-10	3.64E-10	2.67E-10	1.00E-10	9.96E-09	553	4s
	C3	4.06E-08	2.48E-08	1.43E-08	4.06E-08	1.00E-07	6.07E-06	1000	5s
	C4	6.26E-09	3.77E-09	7.59E-09	6.26E-09	1.00E-09	9.67E-08	513	3s
S6	C1	6.53E-09	5.35E-09	7.49E-09	6.53E-09	1.00E-10	9.68E-07	523	2s
	C2	6.52E-09	6.89E-09	7.51E-09	6.52E-09	1.00E-08	9.98E-08	541	3s
	C3	6.70E-10	6.12E-10	8.92E-10	6.70E-10	1.00E-09	1.55E-07	1000	6s
	C4	9.29E-10	9.43E-10	8.66E-10	9.29E-10	1.00E-09	9.96E-08	881	4s

(Source: Self/Authors' Own Illustration)

Figures 8-11 present the graphical solutions of the 2D-MHDSF-MWNF model by LMBM which show the effects for the different physical parameters of the parameter for magnetic (*M*), thermal relaxation constant (*b*), Prandtl number (*Pr*), activation energy (*E*), the reaction rate (*A*), and bio-convection Lewis number (*Lb*) on the functions for flow velocity $f'(\eta)$, fluid temperature $\theta(\eta)$, fluid concentration $\phi(\eta)$, and motile density $\chi(\eta)$.

Figures 8(a-d) display the behavior of the velocity of flow $f'(\eta)$, temperature of fluid $\theta(\eta)$, concentration (η) , and motile density $\chi(\eta)$ profiles affected by the parameter of magnetic (M). When the magnetic parameter is more significant, the velocity decreases, but the fluid temperature, concentration fluid, and motile density are rising.

The action of the thermal relaxation constant on the temperature function is shown in Figure 9(a). By raising the value of the thermal relaxation constant, the temperature is decreasing. Figure 9(b) illustrates the temperature function influenced by the Prandtl number.

The temperature is decreasing by increasing the Prandtl number. Figure 10(a) represents the growing performance for concentration for the increasing activation energy parameter. Figure 10(b) introduces the concentration function affected by the reaction rate. For large values of the reaction rate, the fluid concentration is declining. The decreasing behavior for motile density for variation values of bio-convection Lewis number is displayed in Figure 11. The increased diffusivity for microorganisms caused by the growing bio-convection Lewis number results suggest a decreased motile density.

Figure 8: *The velocity, temperature, concentration, and motile density profiles affected by the magnetic constant*

(a). The f'(η) affected by M   *(b). The θ(η) affected by M*

(c). The φ(η) affected by M   *(d). The χ(η) affected by M*
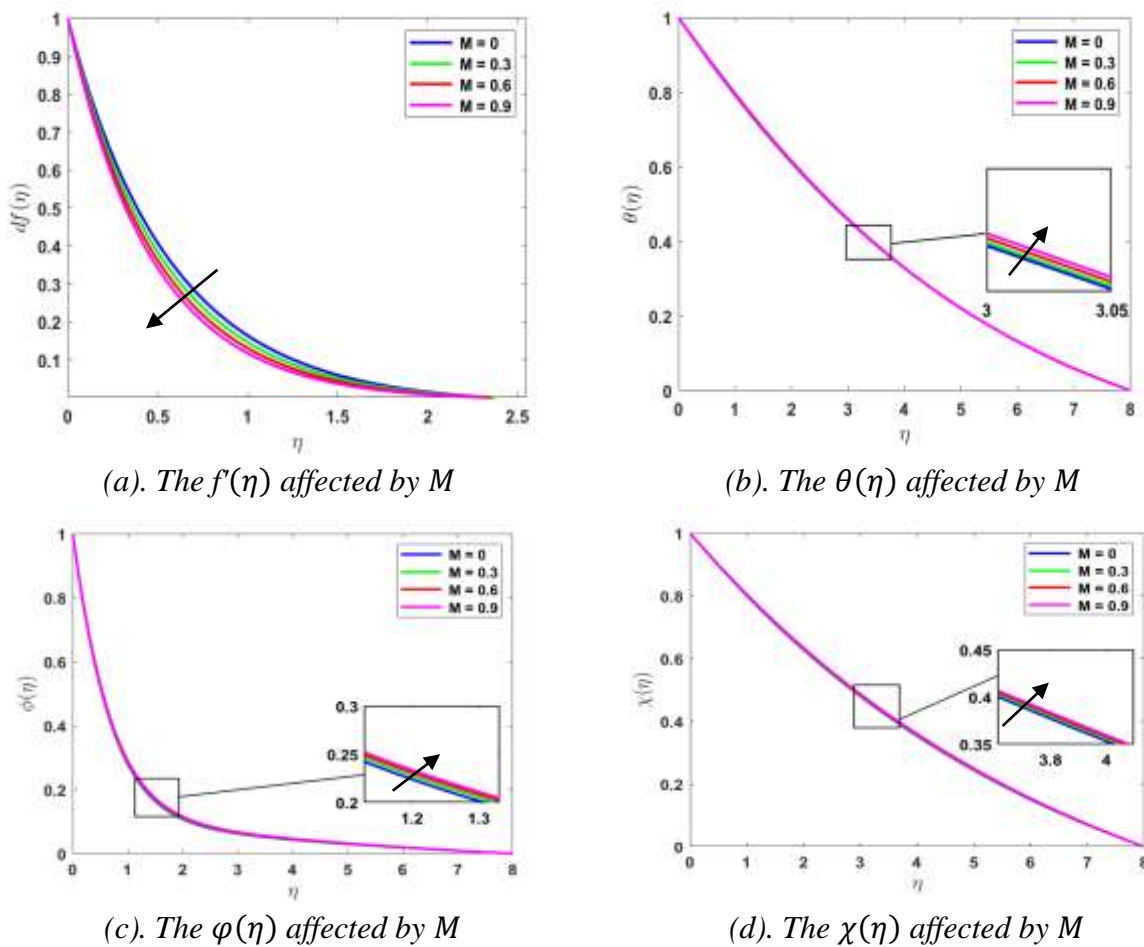
(Source: Self/Authors' Own Illustration)

Figure 9: *The temperature profile affected by Prandtl number and thermal relaxation constant*
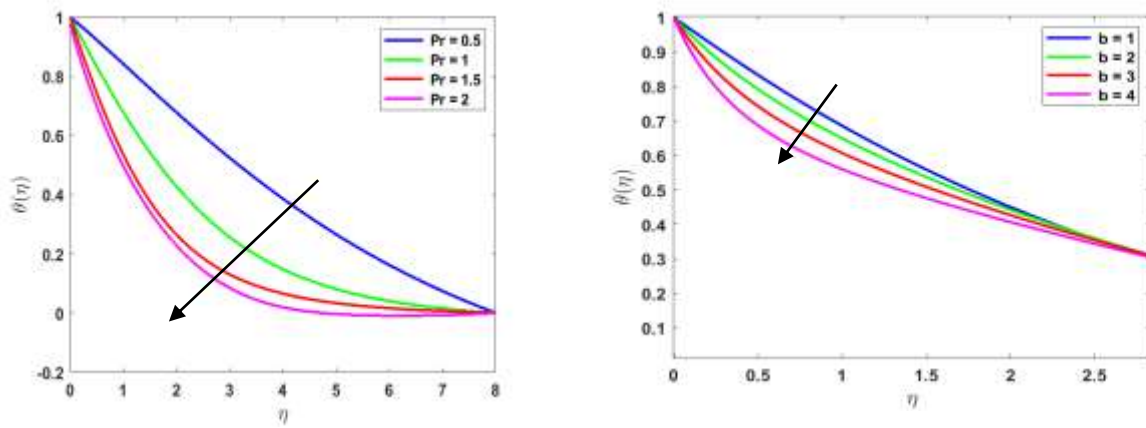
(a). The $\theta(\eta)$ affected by Pr   *(b). The $\theta(\eta)$ affected by b*

Figure 10: *The concentration profile affected by activation energy and reaction rate*
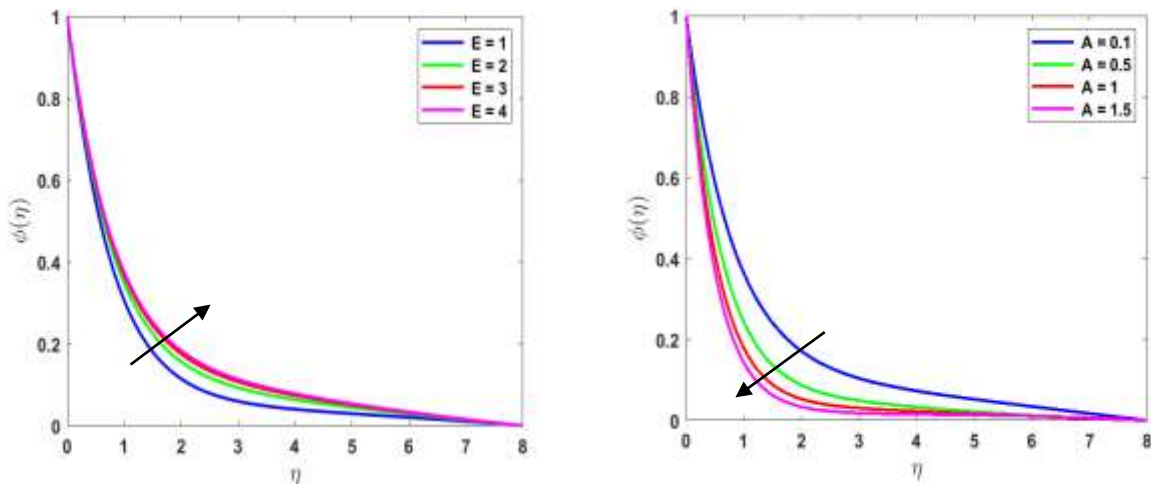
(a). The $\phi(\eta)$ affected by E   *(b). The $\phi(\eta)$ affected by A*

(Source: Self/Authors' Own Illustration)

Figure 11: *The motile density affected by the bio-convection Lewis number*
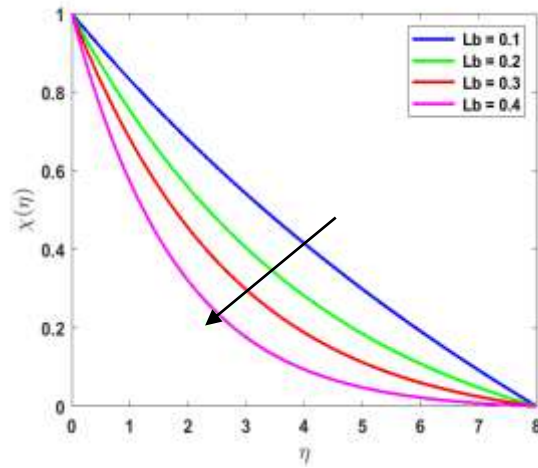

(Source: Self/Authors' Own Illustration)

5. Conclusion and Recommendations

The Levenberg-Marquardt backpropagation method LMBM was used in this work for studying the two-dimensional magnetohydrodynamic stretched flow 2D-MHDSF of Maxwell Williamson nanofluid MWNF influenced by activation energy and bioconvection. The non-linear partial differential equations PDEs system for the 2D-MHDSF-MWNF model was transmuted into a non-linear ordinary differential equations ODEs system. The Lobatto IIIA technique was used to construct reference data which was used to apply LMBM by solving ODEs for different physical parameters. The convergence of LMBM for 2D-MHDSF-MWNF is analyzed through MSE for training, validation, and testing, gradient results, Mu parameter values, histogram of error outcomes, and regression evaluation. The velocity of flow, temperature of fluid, concentration, and motile density behavior affected by various physical variables are presented. The basic outcomes of this study are

- The convergence of the designed LMBM for 2D-MHDSF-MWNF is shown through the gradient outcomes and Mu variable values.
- The accuracy of the proposed LMBM for 2D-MHDSF-MWNF is represented through the MSE for training, validation, and testing steps.
- The stream velocity is decreasing by the magnetic parameter.
- The distribution of the temperature decreases for a larger value of the Prandtl number and thermal relaxation constant while it is growing by the parameter of magnetic.

- The rising value for the activation energy parameter and the parameter of magnetic leads to an increase in the concentration, while the increase in reaction rate tends to decrease the concentration.

- The microorganism motile density is enhanced for high values of magnetic parameter, but it is decreasing for large the bio-convection Lewis number.

- In the future, analyze the effect of the energy activation on various nano-fluidic models ((Abbasi et al., 2022), (Shahid, Bhatti, Ellahi, & Mekheimer, 2022), (Azam, Mabood, & Khan, 2022), (Habib et al., 2022)) by applying the proposed method LMBM.

REFERENCES

Abbasi, A., Khan, S. U., Al-Khaled, K., Khan, M. I., Farooq, W., Galal, A. M., ... & Malik, M. Y. (2022). Thermal prospective of Casson nano-materials in radiative binary reactive flow near oblique stagnation point flow with activation energy applications. Chemical Physics Letters, 786, 139172. https://doi.org/10.1016/j.cplett.2021.139172

Abdal, S., Siddique, I., Alrowaili, D., Al-Mdallal, Q., & Hussain, S. (2022). Exploring the magnetohydrodynamic stretched flow of Williamson Maxwell nanofluid through porous matrix over a permeated sheet with bioconvection and activation energy. Scientific reports, 12(1), 278. https://doi.org/10.1038/s41598-021-04581-1

Abro, K. A., Soomro, M., Atangana, A., & Gómez-Aguilar, J. F. (2020). Thermophysical properties of Maxwell nanofluids via fractional derivatives with regular kernel. Journal of Thermal Analysis and Calorimetry, 1-11. https://doi.org/10.1007/s10973-020-10287-9

Ahmad, A., Sulaiman, M., Alhindi, A., & Aljohani, A. J. (2020). Analysis of temperature profiles in longitudinal fin designs by a novel neuroevolutionary approach. IEEE Access, 8, 113285-113308. https://doi.org/10.1109/ACCESS.2020.3003253

Ahmad, F., Gul, T., Khan, I., Saeed, A., Selim, M. M., Kumam, P., & Ali, I. (2021). MHD thin film flow of the Oldroyd-B fluid together with bioconvection and activation energy. Case Studies in Thermal Engineering, 27, 101218. https://doi.org/10.1016/j.csite.2021.101218

Ahmad, I., Faisal, M., Javed, T., Mustafa, A., & Kiyani, M. Z. (2022). Numerical investigation
for mixed convective 3D radiative flow of chemically reactive Williamson nanofluid
with power law heat/mass fluxes. Ain Shams Engineering Journal, 13(1), 101508.
https://doi.org/10.1016/j.asej.2021.05.022

Ahmed, J., Khan, M., & Ahmad, L. (2020). Radiative heat flux effect in flow of Maxwell
nanofluid over a spiraling disk with chemically reaction. Physica A: Statistical
Mechanics and Its Applications, 551, 123948.
https://doi.org/10.1016/j.physa.2019.123948

Alim, M. A., Alam, M. M., & Hossain, B. (2008). Combined effect of viscous dissipation and
Joule heating on the coupling of conduction and free convection along a vertical flat
plate. International communications in heat and mass transfer, 35(3), 338-346.
https://doi.org/10.1016/j.icheatmasstransfer.2007.06.003

Alsallami, S. A., Zahir, H., Muhammad, T., Hayat, A. U., Khan, M. R., & Ali, A. (2022).
Numerical simulation of Marangoni Maxwell nanofluid flow with Arrhenius activation
energy and entropy anatomization over a rotating disk. Waves in random and complex
media, 1-19. https://doi.org/10.1080/17455030.2022.2045385

Arain, M. B., Zeeshan, A., Alhodaly, M. S., Fasheng, L., & Bhatti, M. M. (2022). Bioconvection
nanofluid flow through vertical rigid parallel plates with the application of Arrhenius
kinetics: A numerical study. Waves in Random and Complex Media, 1-18.
https://doi.org/10.1080/17455030.2022.2123115

Azam, M., Mabood, F., & Khan, M. (2022). Bioconvection and activation energy dynamisms on
radiative sutterby melting nanomaterial with gyrotactic microorganism. Case Studies
in Thermal Engineering, 30, 101749. https://doi.org/10.1016/j.csite.2021.101749

Bhatti, M. M., Arain, M. B., Zeeshan, A., Ellahi, R., & Doranehgard, M. H. (2022). Swimming
of Gyrotactic Microorganism in MHD Williamson nanofluid flow between rotating
circular plates embedded in porous medium: Application of thermal energy storage.
Journal of Energy Storage, 45, 103511. https://doi.org/10.1016/j.est.2021.103511

Buongiorno, J. (2006). Convective transport in nanofluids. https://doi.org/10.1115/1.2150834

Cheema, T. N., Raja, M. A. Z., Ahmad, I., Naz, S., Ilyas, H., & Shoaib, M. (2020). Intelligent
computing with Levenberg–Marquardt artificial neural networks for nonlinear system

of COVID-19 epidemic model for future generation disease control. The European Physical Journal Plus, 135, 1-35. https://doi.org/10.1140/epjp/s13360-020-00910-x

Choi, S. U., & Eastman, J. A. (1995). Enhancing thermal conductivity of fluids with nanoparticles (No. ANL/MSD/CP-84938; CONF-951135-29). Argonne National Lab., IL (United States), 1.

Chu, Y. M., Khan, M. I., Khan, N. B., Kadry, S., Khan, S. U., Tlili, I., & Nayak, M. K. (2020). Significance of activation energy, bio-convection and magnetohydrodynamic in flow of third grade fluid (non-Newtonian) towards stretched surface: A Buongiorno model analysis. International communications in heat and mass transfer, 118, 104893. https://doi.org/10.1016/j.icheatmasstransfer.2020.104893

Daprà, I., & Scarpi, G. (2007). Perturbation solution for pulsatile flow of a non-Newtonian Williamson fluid in a rock fracture. International Journal of Rock Mechanics and Mining Sciences, 44(2), 271-278. https://doi.org/10.1016/j.ijrmms.2006.07.003

Dhlamini, M., Kameswaran, P. K., Sibanda, P., Motsa, S., & Mondal, H. (2019). Activation energy and binary chemical reaction effects in mixed convective nanofluid flow with convective boundary conditions. Journal of Computational Design and Engineering, 6(2), 149-158. https://doi.org/10.1016/j.jcde.2018.07.002

Esfe, M. H., Esfandeh, S., & Hosseinizadeh, E. (2020). Nanofluid flooding for enhanced oil recovery in a heterogeneous two-dimensional anticline geometry. International Communications in Heat and Mass Transfer, 118, 104810. Gowda, R. P., Kumar, R. N., Prasannakumara, B. C., Nagaraja, B., & Gireesha, B. J. (2021). Exploring magnetic dipole contribution on ferromagnetic nanofluid flow over a stretching sheet: An application of Stefan blowing. Journal of Molecular Liquids, 335, 116215. https://doi.org/10.1016/j.molliq.2021.116215

Gul, T., Usman, M., Khan, I., Nasir, S., Saeed, A., Khan, A., & Ishaq, M. (2021). Magneto hydrodynamic and dissipated nanofluid flow over an unsteady turning disk. Advances in Mechanical Engineering, 13(7), 16878140211034392. https://doi.org/10.1177/16878140211034392

Habib, D., Salamat, N., Abdal, S., Siddique, I., Ang, M. C., & Ahmadian, A. (2022). On the role of bioconvection and activation energy for time dependent nanofluid slip transpiration

due to extending domain in the presence of electric and magnetic fields. Ain Shams Engineering Journal, 13(1), 101519. https://doi.org/10.1016/j.asej.2021.06.005

Hayat, T., Khan, S. A., Khan, M. I., & Alsaedi, A. (2019). Theoretical investigation of Ree–Eyring nanofluid flow with entropy optimization and Arrhenius activation energy between two rotating disks. Computer methods and programs in biomedicine, 177, 57-68. https://doi.org/10.1016/j.cmpb.2019.05.012

Hussain, S. M., Sharma, R., Mishra, M. R., & Alrashidy, S. S. (2020). Hydromagnetic dissipative and radiative graphene maxwell nanofluid flow past a stretched sheet-numerical and statistical analysis. Mathematics, 8(11), 1929. https://doi.org/10.3390/math8111929

Irfan, M., Khan, W. A., Khan, M., & Gulzar, M. M. (2019). Influence of Arrhenius activation energy in chemically reactive radiative flow of 3D Carreau nanofluid with nonlinear mixed convection. Journal of Physics and Chemistry of Solids, 125, 141-152. https://doi.org/10.1016/j.jpcs.2018.10.016

Kanta Mondal, S., & Pal, D. (2022). Gyrotactic mixed bioconvection flow of a nanofluid over a stretching wedge embedded in a porous media in the presence of binary chemical reaction and activation energy. International Journal of Ambient Energy, 43(1), 3443-3453. https://doi.org/10.1080/01430750.2020.1814860

Khan, N. A., Sulaiman, M., Aljohani, A. J., Kumam, P., & Alrabaiah, H. (2020). Analysis of multi-phase flow through porous media for imbibition phenomena by using the LeNN-WOA-NM algorithm. IEEE Access, 8, 196425-196458. https://doi.org/10.1109/ACCESS.2020.3034053

Khan, N. A., Sulaiman, M., Kumam, P., & Aljohani, A. J. (2021). A new soft computing approach for studying the wire coating dynamics with Oldroyd 8-constant fluid. Physics of Fluids, 33(3). https://doi.org/10.1063/5.0042676

Khan, W. A., & Makinde, O. D. (2014). MHD nanofluid bioconvection due to gyrotactic microorganisms over a convectively heat stretching sheet. International Journal of Thermal Sciences, 81, 118-124. https://doi.org/10.1016/j.ijthermalsci.2014.03.009

Krishnamurthy, M. R., Prasannakumara, B. C., Gireesha, B. J., & Gorla, R. S. R. (2016). Effect of chemical reaction on MHD boundary layer flow and melting heat transfer of

Williamson nanofluid in porous medium. Engineering Science and Technology, an International Journal, 19(1), 53-61. https://doi.org/10.1016/j.jestch.2015.06.010

Lira, J. O., Riella, H. G., Padoin, N., & Soares, C. (2022). Computational fluid dynamics (CFD), artificial neural network (ANN) and genetic algorithm (GA) as a hybrid method for the analysis and optimization of micro-photocatalytic reactors: NOx abatement as a case study. Chemical Engineering Journal, 431, 133771. https://doi.org/10.1016/j.cej.2021.133771

Mustafa, M., Khan, J. A., Hayat, T., & Alsaedi, A. (2017). Buoyancy effects on the MHD nanofluid flow past a vertical surface with chemical reaction and activation energy. International Journal of Heat and Mass Transfer, 108, 1340-1346. https://doi.org/10.1016/j.ijheatmasstransfer.2017.01.029

Noreen, S., Waheed, S., Lu, D. C., & Hussanan, A. (2020). Heat measures in performance of electro-osmotic flow of Williamson fluid in micro-channel. Alexandria Engineering Journal, 59(6), 4081-4100. https://doi.org/10.1016/j.aej.2020.07.013

Raees, A., Xu, H., Sun, Q., & Pop, I. (2015). Mixed convection in gravity-driven nano-liquid film containing both nanoparticles and gyrotactic microorganisms. Applied Mathematics and Mechanics, 36(2), 163-178. https://doi.org/10.1007/s10483-015-1901-7

Rashid, M., Ansar, K., & Nadeem, S. (2020). Effects of induced magnetic field for peristaltic flow of Williamson fluid in a curved channel. Physica A: Statistical Mechanics and its Applications, 553, 123979. https://doi.org/10.1016/j.physa.2019.123979

Rasool, G., Chamkha, A. J., Muhammad, T., Shafiq, A., & Khan, I. (2020). Darcy-Forchheimer relation in Casson type MHD nanofluid flow over non-linear stretching surface. Propulsion and Power Research, 9(2), 159-168. https://doi.org/10.1016/j.jppr.2020.04.003

Reddy, S. R. R., Reddy, P. B. A., & Bhattacharyya, K. (2019). Effect of nonlinear thermal radiation on 3D magneto slip flow of Eyring-Powell nanofluid flow over a slendering sheet with binary chemical reaction and Arrhenius activation energy. Advanced Powder Technology, 30(12), 3203-3213. https://doi.org/10.1016/j.apt.2019.09.029

Shahid, A., Bhatti, M. M., Ellahi, R., & Mekheimer, K. S. (2022). Numerical experiment to examine activation energy and bi-convection Carreau nanofluid flow on an upper

paraboloid porous surface: Application in solar energy. Sustainable Energy
Technologies and Assessments, 52, 102029.
https://doi.org/10.1016/j.seta.2022.102029

Sharif, H., Naeem, M. N., Khadimallah, M. A., Ayed, H., Bouzgarrou, S. M., Al Naim, A. F., ...
& Tounsi, A. (2020). Energy effects on MHD flow of Eyring's nanofluid containing
motile microorganism. Advances in concrete construction, 10(4), 357-367.

Sharma, R., Hussain, S. M., Raju, C. S. K., Seth, G. S., & Chamkha, A. J. (2020). Study of
graphene Maxwell nanofluid flow past a linearly stretched sheet: A numerical and
statistical approach. Chinese Journal of Physics, 68, 671-683.
https://doi.org/10.1016/j.cjph.2020.10.013

Sreedevi, P., Sudarsana Reddy, P., & Chamkha, A. (2020). Heat and mass transfer analysis of
unsteady hybrid nanofluid flow over a stretching sheet with thermal radiation. SN
Applied Sciences, 2(7), 1222. https://doi.org/10.1007/s42452-020-3011-x

Shoaib, M., Naz, S., Nisar, K. S., Raja, M. A. Z., Aslam, S., & Ahmad, I. (2023). MHD casson
nanofluid in darcy-forchheimer porous medium in the presence of heat source and
arrhenious activation energy: applications of neural networks. International Journal of
Modelling and Simulation, 43(4), 438-461.
https://doi.org/10.1080/02286203.2022.2091973

Zeeshan, A., Arain, M. B., Bhatti, M. M., Alzahrani, F., & Bég, O. A. (2022). Radiative
bioconvection nanofluid squeezing flow between rotating circular plates: Semi-
numerical study with the DTM-Padé approach. Modern Physics Letters B, 36(03),
2150552. https://doi.org/10.1142/S0217984921505527

Sources:

- **Figure 1. (Source: Abdal et al., 2022).**
- **All another figures and tables. (Source: Self/Authors' Own Illustration).**

Nomenclature:

ANN	Artificial Neural Networks	MHDSF	Magnetohydrodynamic stretched flow
2D-MWNF	two-dimensional Maxwell Williamson nanofluid	LMBM	Levenberg-Marquardt backpropagation method
PDE	A partial differential equation	ODE	An ordinary differential equation
(u, v)	The velocity components	MSE	Mean squared error
(x, y)	The cartesian coordinates	u_w	Wall constant velocity
B_0	Magnetic field constant	C	The concentration
T	The temperature of the fluid	σ	Electrical conductivity
k	The fluid parameter	C_p	The heat at constant pressure
k_1	Permeability of porous medium	D_T	The thermophoresis diffusion parameter
(τ_1, τ_2)	Heat flux relaxation time	C_∞	Free flow concentration
T_∞	Free flow temperature	R	Thermal radiation parameter
α	Thermal diffusivity of base fluid	m	Power law index
D_B	The Brownian diffusion parameter	T_w	The temperature of fluid on the wall
W_e	Local Weissenberg number	C_w	The concentration on the wall
υ	Viscosity kinematic	N	Density of microorganisms
ρ	Fluid density	ρ_p	Density of nanoparticle
γ	Spin gradient viscosity	η	Similarity variable

θ	Dimensionless temperature function	μ	Viscosity of fluid
Nr	buoyancy ratio	*f*	Dimensionless flow function
φ	Dimensionless concentration function	*S1* *C1*	Scenario 1,…, etc Case 1,…, etc